Selective targeting of the retinal pigment epithelium using an acousto-optic laser scanner

Clemens Alt
Massachusetts General Hospital
Harvard Medical School
Wellman Center for Photomedicine
Boston, Massachusetts 02114
and
Tufts University
Department of Biomedical Engineering
Medford, Massachusetts

Carsten Framme
Massachusetts General Hospital
Harvard Medical School
Wellman Center for Photomedicine
Boston, Massachusetts 02114
and
Medical Laser Center Lübeck
Lübeck, Germany
and
University Eye Hospital Regensburg
Regensburg, Germany

Susanne Schnell
Massachusetts General Hospital
Harvard Medical School
Wellman Center for Photomedicine
Boston, Massachusetts 02114
and
University of Applied Sciences
Hamburg
Hamburg, Germany

Ho Lee
Massachusetts General Hospital
Harvard Medical School
Wellman Center for Photomedicine
Boston, Massachusetts 02114

Ralf Brinkmann
Medical Laser Center Lübeck
Lübeck, Germany

Charles P. Lin
Massachusetts General Hospital
Harvard Medical School
Wellman Center for Photomedicine
Boston, Massachusetts 02114
E-mail: lin@helix.mgh.harvard.edu

Abstract. Selective targeting of the retinal pigment epithelium (RPE) is a new strategy for treating certain retinal disorders while preserving adjacent photoreceptors. The treatment currently relies on a complex laser system to produce the required microsecond pulse structure. In our new approach, we scan the focus of a continuous-wave (cw) laser beam with acousto-optic deflectors to produce microsecond-long exposures at each RPE cell. Experiments were performed *in vitro* with a bench-top scanner on samples of young bovine RPE and *in vivo* on Dutch belted rabbits with a slit-lamp adapted scanner. Effective dose 50% (ED_{50}) for RPE damage was determined *in vitro* by fluorescence cell viability assay and *in vivo* by fluorescein angiography. Damage to individual RPE cells was achieved with laser power on the order of 100 mW. Using separated scan lines, we demonstrate selectivity in the form of alternating lines of dead and surviving cells that resemble the scan pattern. Selectivity is also shown by the absence of retinal thermal coagulation *in vivo*. Selective RPE damage is feasible by rapidly scanning a cw laser beam. The scanning device is an attractive alternative to conventional laser coagulation and pulsed laser targeting of the RPE.
[DOI: 10.1117/1.2136314]

Keywords: retinal pigment epithelium; selective laser treatment; laser scanning; central serous retinopathy; age-related macular degeneration; diabetic macular edema.

Paper 05063R received Mar. 7, 2005; revised manuscript received Jun. 22, 2005; accepted for publication Jun. 23, 2005; published online Nov. 23, 2005. This paper is a revision of a paper presented at the SPIE conference on Ophthalmic Technologies XII, Jan. 2002, San Jose, CA. The paper presented there appears (unrefereed) in SPIE Proceedings Vol. 4611.

1 Introduction

Laser photocoagulation is a well-established treatment modality for a variety of retinal disorders and is commonly used in ophthalmic clinics worldwide. Conventional retinal laser coagulation is usually performed using an argon ion (514 nm) or a green solid-state laser. Exposure times typically range from 50 to 200 ms. Earlier studies have shown that a variety of retinal diseases such as retinal detachment and diabetic retinopathy are treated successfully by conventional laser co-

Address all correspondence to Clemens Alt. Wellman Center for Photomedicine, MGH/BAR822, 55 Fruit Street, Boston, MA 02114. Tel: 617-726-4962; Fax: 617-724-2075; E-mail: alt@helix.mgh.harvard.edu

1083-3668/2005/10(6)/064014/11/$22.00 © 2005 SPIE

agulation. The benefit for the patient, however, has to be considered very carefully when performing macular irradiation. Following the thermal destruction of the retinal pigment epithelium (RPE), which is the primary absorption site, an irreversible coagulation of the neural retina occurs due to heat diffusion[1–4] and will most likely result in laser scotomas, which could lead to a severe loss of visual acuity. This effect is manifested ophthalmoscopically as a visible grayish-white lesion.

The RPE is a single cell layer adjacent to the outer segments of the photoreceptors. Together with Bruch's membrane, it forms the outer blood ocular barrier that separates the neurosensory tissue from the choroidal vasculature.[5] The RPE regulates molecular transport to and from the photoreceptors and is responsible for phagocytosis of the shed photoreceptor outer segments.[5] Certain macular diseases such as diabetic macular edema, drusen, and central serous retinopathy are thought to be associated with dysfunction of the RPE. Although RPE cells do not regenerate under normal circumstances,[6,7] they can proliferate and migrate to cover the laser lesion following laser treatment.[7,8] It has been shown that lesions are fully covered after 14 days by new RPE cells.[8] Recovery of RPE re-establishes the blood-retinal barrier and may facilitate the removal of existing edema or drusen. Such a proposed healing effect does not require thermal denaturation of the neuroretina. Therefore, a method for selectively injuring the RPE cells, without causing adverse effects to choriocapillaris and to the photoreceptors, should be an appropriate treatment for retinal diseases that are mainly associated with dysfunction of the RPE.[8]

Selective photothermolysis is described as a process in which the transfer of laser energy is restricted to a particular, selectively absorbing site. Appropriate selection of a therapeutic wavelength that is preferentially absorbed by a target chromophore, and choice of exposure time that is comparable to or shorter than the thermal relaxation time of that absorber, can lead to selective destruction of highly absorbing target tissue, while surrounding less absorbing tissue is preserved.[9]

The RPE is an ideal model to test the ability to selectively target a single cell layer that is loaded with highly absorbing chromophores (melanosomes) and is situated in close proximity to a very sensitive, but less absorbing, cell layer (the photoreceptors). The RPE layer absorbs about 50% of incident green light, compared to less than 10% absorption by the photoreceptors.[10] Selective RPE targeting was first demonstrated by Birngruber and Roider in rabbits using repetitive argon laser pulses at 514 nm with pulse durations of 5 μs and a repetition rate of 500 Hz.[8] By irradiating the fundus with a train of repetitive laser pulses, at durations close to the thermal confinement time of the RPE cells, it is possible to achieve high peak temperatures around the melanosomes. Only a low, sublethal background temperature increase occurs outside the RPE cells, and thus the adjacent tissue structures are spared from thermal damage.[11] Because of the lack of thermal coagulation, these effects are ophthalmoscopically invisible but can be visualized by angiography. Selective destruction of RPE cells was further demonstrated in animal studies, using various exposure times between 5 μs and 200 ns, by histological examinations at different time points post-treatment. Microperimetry in human eyes treated with 1.7-μs pulse duration show photoreceptor function over the treatment sites.[12,13]

Despite those successful demonstrations, selective RPE targeting remains an experimental procedure, largely because of the lack of a clinically viable laser source that is compact, simple to maintain, and capable of generating the required microsecond pulse structure. The aim of our study was to investigate whether selective RPE laser treatment can be achieved by using a simple cw laser that is focused to a small spot and rapidly scanned over the retina, so as to produce an effective microsecond pulse at each exposed RPE cell. Such a device will be more compact and more versatile than the existing pulsed approach prototype.[14] Brinkmann et al. reported an initial scanning experiment performed *in vitro* using a multimode-fiber coupled cw argon laser.[15] We describe both *in vitro* and *in vivo* (rabbit) feasibility experiments using a scanning device that employs Gaussian beam characteristics from a cw laser source.

2 Material and Methods

2.1 *Scanner Design*

A 2-D acousto-optic deflector (AOD) was used to generate the scan pattern in both the *in vitro* and *in vivo* setups. In an AOD, maximum intensity of diffracted light in the first-order beam occurs when the Bragg condition is satisfied. An acoustic wave propagating through a crystal creates a sinusoidal change of its optical index. The incident collimated laser beam then "sees" an optical diffraction grating, where the acoustic wavelength determines the grating width. Sweeping the acoustic frequency by an electrical signal changes the grating width, yielding a sweeping scan angle and thus, a moving spot. Mounting two AOD crystals perpendicular to each other into one package then creates a 2-D scan pattern.

To control our 2-D AOD (2DS-100-35-.532, Brimrose, Baltimore, Maryland), four electric signals are needed (Fig. 1): one frequency modulation (FM) signal per crystal or scan axis, respectively, an amplitude modulation (AM) signal to enable the first-order beam, and a trigger pulse to synchronize the control unit.

A two-channel, arbitrary function generator (Tektronix, AFG320) creates the two custom-programmed FM signals. Utilizing the four fixed memories for arbitrary waveforms of the generator, the user is able to switch back and forth between different characteristics of the scan pattern. The AM signal is generated by a window comparator. Our home-built window comparator switches AM ON, when the FM_1 voltage crosses the lower voltage set point that determines the left edge of the scan field. Likewise, it switches AM OFF, when FM_1 crosses the higher FM_1 reference voltage that corresponds to the right edge of the scan field (Fig. 2). This enables the user to switch between different characteristics of the scan pattern without changing its size. For instance, it is sufficient to change the slew rate of the FM_1 ramp signal to produce a different scan speed. To define the repetition frequency (frame rate) of the scan pattern and the number of repetitions applied to each irradiation site, an additional digital pulse generator (Tektronix, PFG5105) is used to trigger the entire control unit. With this control design, we were able to produce two basic shapes of a scan pattern: one that is composed of six separated

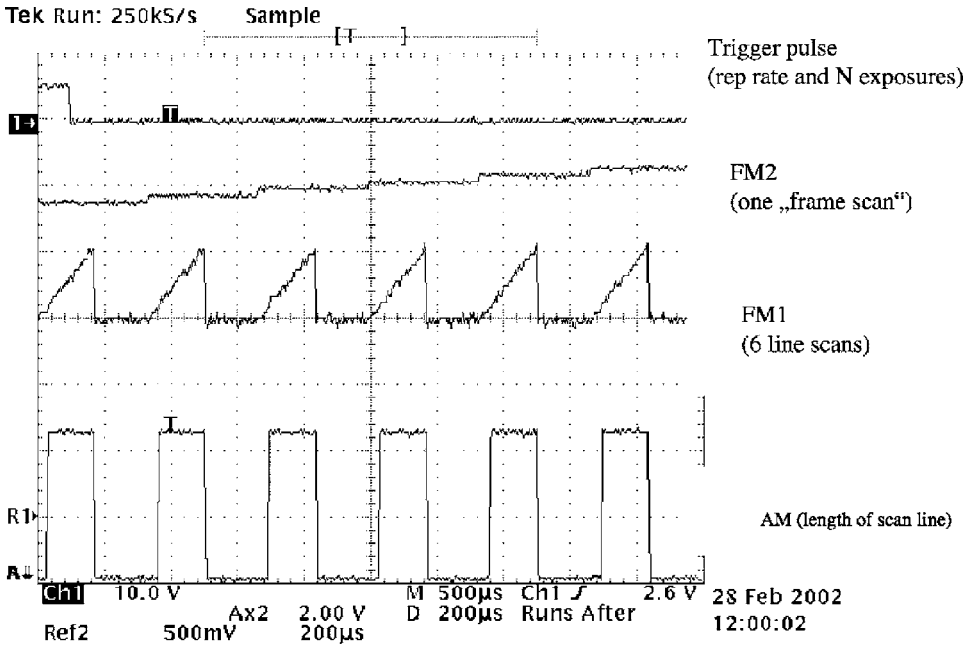

Fig. 1 Electrical command signals employed to create one scan pattern with separated lines with the 2-DAOD in our application. FM_1 deflects the light fast but with a constant speed (horizontal line scan). A second, slower FM_2 steps the spot into the position where the next line is to be produced (vertical frame scan). To switch the first-order beam on and off to sharply define the edges of the scan lines, the AM signal is applied in parallel to both crystals. A trigger pulse synchronizes the control unit and defines repetition rate and number of patterns to be created in one cycle.

lines (SEP) and a second consisting of 21 interlaced lines (INT) without spacing between lines (Fig. 2).

Both scanners are aligned in such a way that the central acoustic frequency of the full bandwidth of the 2-D AOD defines the optical axis of each device. The scan angles for the line and the frame scans are produced as half angles around this optical axis to minimize coma, which may occur due to any scanning process, as the beam by default is steered off the optical axis. To focus the first-order beam, a single achromatic lens was placed one focal distance from the midpoint between the two crystals of the 2-D AOD, forming a nearly telecentric optic, to minimize curvature of the scanners' focal plane.

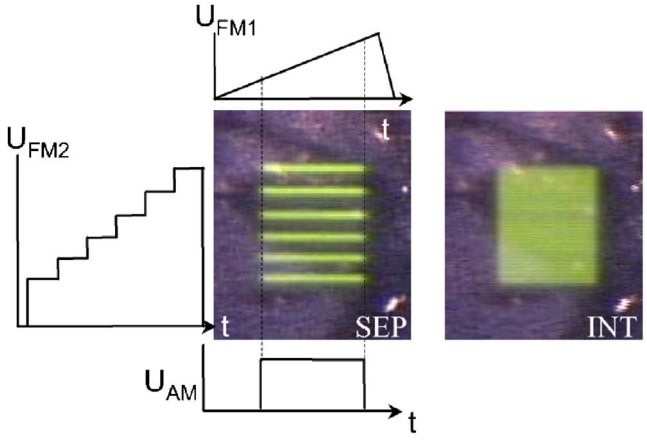

Fig. 2 Two patterns of the *in vivo* scanning device. On the left is the separated lines scan pattern (SEP) with cartoons of its accompanying control signals (Fig. 1). The dashed vertical lines mark the low and high reference voltages of FM_1 that define the left and right edges of the pattern; they are utilized to switch the AM signal on and off. The pattern on the right is an interlacing scan pattern (INT). It produces, similar to the SEP pattern, three patterns of seven separated lines that are spatially displaced by one line.

The spot diameters and beam profiles of the setups were determined on a stationary spot centered in the scan pattern using the knife-edge method along (x), at 45 deg and perpendicular (y) to the direction of motion of the line scan. A 200-μm-wide slit was mounted a known distance from the axle on a rotating wheel. While spinning the wheel at a carefully monitored frequency, the rise and fall time of the signal behind the two edges of the slit were measured to determine the spot size. Three measurement runs per orientation were conducted to compute mean diameter and error. For profiling, the average rise time signals were differentiated. The scan speed was measured by scanning the laser spot along a microscope scale (100 div/1 mm), detecting the transmitted light with a photodiode and measuring the time between two minima produced when the spot runs over a cross-hair of the scale.

2.2 *Determination of Threshold Exposure*

Both *in vitro* and *in vivo* devices were used to determine the effective dose 50% (ED_{50}) for RPE cell damage. ED_{50} describes a probability of 50% that an exposed cell will be killed. ED_{50} was determined by Probit analysis for individual samples *in vitro* and individual eyes *in vivo*.

In Probit analysis, the cumulative density distribution of the percentage of targets that do respond to a given dose is plotted versus the dose that was applied. The program (Probit, Version 2.1.1) produces a lognormal fit through the quantal response data, which are represented by 1 for success and 0 for no success. As a result, a probability function versus the dose is being calculated and the ED_{50} determined.[16]

Table 1 Slopes of the probability distribution of *in vitro* experiments on sheets of RPE. Here, the slope is defined as the ratio of ED_{85}/ED_{50}. All measurements were performed in duplicates and the data listed are the average values.

Repetition frequency	Parameter	ED_{50} (mW)	ED_{15} (mW)	ED_{85} (mW)	Slope
100 Hz	3 μs, N=10	221	212	230	1.04
	3 μs, N=100	206	201	210	1.02
	10 μs, N=10	130	126	135	1.04
500 Hz	3 μs, N=10	222	216	228	1.03
	3 μs, N=100	182	180	184	1.01
	10 μs, N=10	130	126	135	1.04

The endpoint for experiments on RPE sheets *in vitro* was the appearance of lines of dead cells according to a viability assay that is described in Sec. 2.3.2. If lines in a lesion were partially damaged, i.e., if it was questionable whether to assign a 0 or a 1 to that lesion, the number of dead cells in a scan line was counted. Since about 20 RPE cells fit into the length of one scan line, lesions with fewer than 10 cells per line constitute a 0 for Probit analysis, and lesions with more than 10 cells per line constitute a 1.

The endpoint for *in vivo* experiments in rabbit eyes was the appearance of hyperfluorescent lesions in fluorescence angiography, as described in Sec. 2.4.4.

Results are presented for each set of parameters as the average ED_{50} and the absolute deviation of ED_{50} from individual samples or eyes. The slope of the probability distribution, defined as the ratio of ED_{85} over ED_{50}, is also presented in Table 1 for *in vitro* experiments on sheets of RPE and in Table 2 for *in vivo* experiments in rabbit eyes.

2.3 *In Vitro Experiments*

2.3.1 *Setup*

The *in vitro* scanner was assembled using the design described earlier. It produced a scan pattern of 300×300 μm with spacing of 60 μm between line centers. A 5-W cw laser (VERDI, Coherent, Saint Clara, California) served as laser source for the irradiation. An argon ion laser (INNOVA 90, Coherent) at 488 nm, delivered through a multimode fiber, was used for excitation of the fluorescent cell viability probe, as described later. A custom-built compound fluorescence microscope was set up to capture fluorescence images before and after irradiation (Fig. 3).

2.3.2 *Samples and viability marker*

RPE sheets from young bovine eyes were used for *in vitro* experiments. Samples were exposed to various levels of laser power using the separated lines scan pattern (SEP). Feasibility was tested with two different scan speeds, producing exposure times per cell of 3 and 10 μs. Ten and 100 repetitive exposures were applied with repetition frequencies of 100 and 500 Hz for each exposure time. All measurements were performed in duplicates.

One sample of roughly 15 mm diameter was prepared from the posterior segment of each eye. After removal of the neuroretina, the sample was incubated in CalceinAM (Molecular Probes, Eugene, OR). CalceinAM is a nonfluorescent dye. Because it is also nonpolar, it diffuses into cells where it is reduced by esterase to Calcein, which performs as the actual fluorescence marker. The spectrum of Calcein shows an excitation peak at a wavelength of 490 nm and an emission maximum at 520 nm.[17] Calcein is polar, and thus is unable to leave the cells. Live cells therefore will appear bright under fluorescence illumination conditions, whereas dead cells, whose membrane integrity has been compromised, will appear dark.

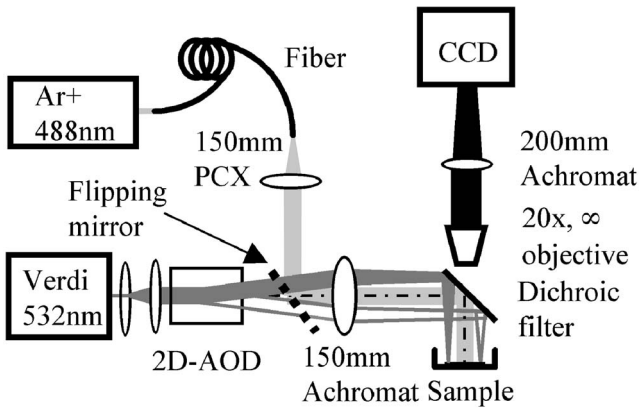

Fig. 3 Schematic of the bench-top *in vitro* setup. The output beam of the diode-pumped solid-state Verdi was enlarged to the size of the full active aperture of the 2-DAOD (5 mm) with a Keplerian beam expander. After passing the focusing achromat (f.l=150 mm) at the output side of the AOD, the first-order beam was directed vertically by a dichroic filter onto the sample, which was placed horizontally on a 3-D translation stage. A compound fluorescence microscope employing an infinity-corrected 20× objective with a large working distance was erected on top of the dichroic filter and the sample holder to visualize the sample through a CCD camera. A fiber-coupled white light source illuminated the sample (not shown). Radiation from an argon ion laser (488 nm) was coupled into a multimode fiber. The fiber output was introduced into the beam path by a flipping mirror for fluorescence excitation of the viability assay Calcein.

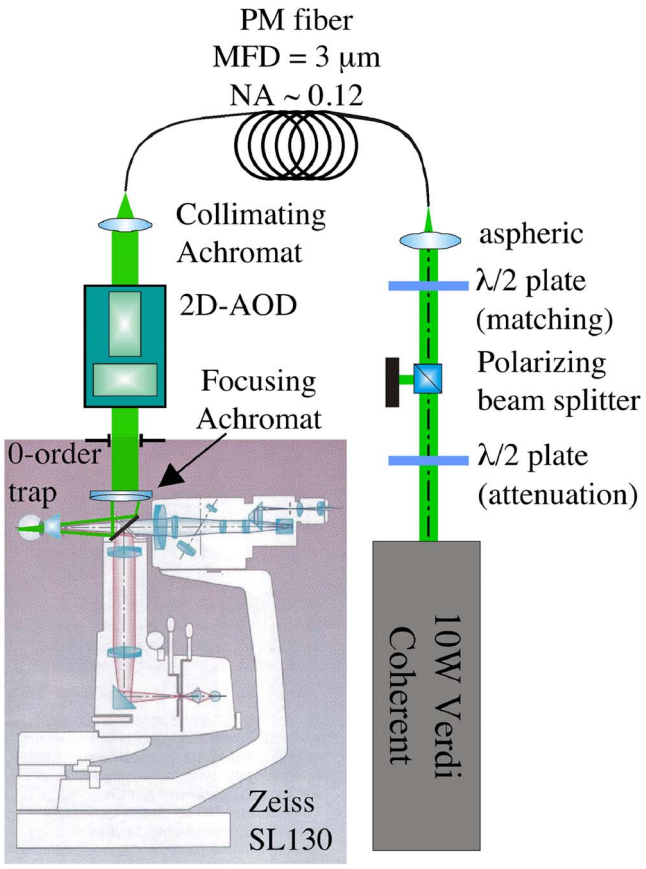

Fig. 4 Schematic of the slit-lamp adapted *in vivo* setup. The output power of the Verdi laser was controlled by an attenuator. An additional λ/2-plate rotated the polarization state of the light into the fast axis of the PM fiber to maintain the highest possible stability of the linear polarization orientation at the output side of the fiber. A single achromatic lens collimated the beam, leaving the PM fiber to the size of the active aperture of the AOD. The focusing lens was placed after the AOD in a nearly telecentric way. The mirror directing the irradiation light away from the slit lamp was placed between the two lenses of the objective of the slit lamp and the two mirrors of the double-slit illumination.

After incubation, the sample was placed in a petri dish. A lid with a hole in the center held the sample in place. The dish was filled with phosphate-buffered saline (PBS) and the opening in the lid closed with a microscope cover glass. After irradiation, a fluorescence image was captured and the damage evaluated according to the viability assay.

2.4 *In Vivo Experiments*

2.4.1 *Setup*

For the *in vivo* experiments, a slit-lamp adapted laser scanner was developed. The emission (532 nm) of a cw laser (VERDI V-10, Coherent) was coupled into a polarization maintaining single-mode fiber (PM fiber) (HB450, Fibercore Limited, United Kingdom). The output power of the Verdi laser was attenuated by combination of a λ/2-plate and a polarizing beamsplitter cube and coupled into the fiber. An additional λ/2-plate matched the polarization state with the fast axis of the PM fiber. Using an attenuator allows the laser to run at constant power at all times and minimizes pointing instabilities. PM fiber was necessary to preserve diffraction-limited beam characteristics and because linear polarization is required for optimal operation of the AOD. Its use limited the power that could be delivered to the setup to about 300 mW. With a typical diffraction efficiency of two AODs (≈64%), the highest possible power entering the eye was 185 mW.

Table 2 Slopes of the probability distribution of *in vivo* experiments. Here, the slope is defined as the ratio of ED_{85}/ED_{50}. All measurements were performed in duplicates and the data listed are the average values.

Parameter	ED_{50} (mW)	ED15 (mW)	ED85 (mW)	Slope
7.5 μs, N=10, SEP	92	89	95	1.03
7.5 μs, N=100, INT	67	62	72	1.08
7.5 μs, N=10, INT	69	64	74	1.08
15 μs, N=10, SEP	66	63	69	1.05
15 μs, N=100, SEP	57	56	59	1.03
15 μs, N=100, INT	45	41	48	1.08

The scanner design described in Sec. 2.1 was mounted with its mechanical components, collimating and focusing optics vertically on top of the slit lamp (SL130, Zeiss, Oberkochen, Germany). The PM fiber output and the collimator were mounted on a six-axis stage (x, y, z, tip, tilt, and rotate) to match the Bragg condition and the preferred polarization direction of the 2-D AOD. A mirror, placed between the two lenses of the stereo objective of the slit lamp, directed the first-order beam horizontally away from the objective into the eye, running along the optical axis of the slit lamp (Fig. 4).

To achieve the same size of the scan pattern on the retina as used in the *in vitro* experiments, the scan field in air was enlarged to a width and height of 450 μm, with 90-μm spacing between line centers for the SEP pattern. The energy to the rabbit eye was applied through a Goldman contact lens, which together with the optics of the rabbit eye, magnifies all distances on the retina by a factor of 0.66,[18] making the scan area 300×300 μm, with 60-μm spacing, on the retina.

2.4.2 *Animals*

Dutch belted rabbits were chosen because the density and location of light-absorbing pigments in the fundus of rabbits are rather uniform and similar to that of the human eye.[10] The animals were anesthetized and placed in a holder system that allowed tilting and rotating of the animal relative to the slit lamp. The contact lens was placed onto the mydriatic eye using methylcellulose 2% as contact gel. The lens was attached to the animal holder by a special clamping system to prevent unfavorable movements.

The treatment of experimental animals in this study was in compliance with the Association for Research in Vision and Ophthalmology Resolution on the Use of Animals in Research.

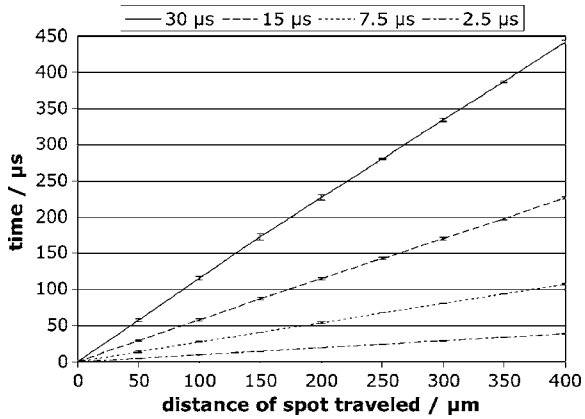

Fig. 5 Demonstration of the scan speed along the line being constant using our AOD. The data shown represent the measurements for 30-, 15-, 7.5-, and 2.5-μs exposures. In this work, the speed is always expressed in terms of its resulting exposure time, that is, the time the spot needs to travel a distance equivalent to its $1/e^2$ diameter.

2.4.3 *Laser treatment and documentation*

Ophthalmoscopically visible marker lesions for orientation were placed in each eye. The selective treatment lesions that are ophthalmoscopically invisible were placed between these marker lesions using different power levels in a predefined grid pattern. A total number of 308 lesions in 12 eyes covered a variety of parameter sets. For each parameter, ED_{50} was determined in two eyes of different individuals.

The repetition frequency for all parameter sets *in vivo* was 100 Hz. For the SEP scan pattern, consisting of six separated lines [Fig. 2(a)], the speed was varied to create 7.5 and 15 μs exposures in the center of the scan line. 10 and 100 repetitions per irradiation site were applied for both scan speeds. For the INT pattern (21 interlacing lines without spacing) [Fig. 2(b)] 10 repetitions of 7.5-μs exposure and 100 repetitions of 15-μs exposure were tested as presumably the least or most invasive parameters, respectively.

2.4.4 *Determination of threshold exposure*

One hour after irradiation, fluorescence angiography was performed by injection of 10% sodium fluorescein into the ear vein. If the RPE is damaged, the blood ocular barrier is compromised and fluorescein can pool from the choriocapillaris into the subretinal space.[19] Under fluorescence illumination, lesions will then appear bright, whereas undamaged areas will remain dark. Thus, fluorescein angiography was used to detect damages of the RPE barrier and identify lesions. ED_{50} values were calculated using Probit analysis. The endpoint was the appearance of angiographically visible lesions.

2.4.5 *Calculation of the radiant exposure*

Integration of a Gaussian irradiance profile, which is being scanned in the x direction, in Cartesian coordinates yields the radiant exposure $H(y)$ for each point at a certain distance y from the center of the scan line when the spot is being moved with a velocity v:[15]

$$H(y) = \sqrt{\frac{2}{\pi}} \cdot \frac{P}{\omega_0 \cdot v} \cdot \exp\left(-\frac{2y^2}{\omega_0^2}\right), \tag{1}$$

where P is the total power, ω_0 the $1/e^2$ radius of the Gaussian profile, and y is the distance from the center of the scan line perpendicular to the direction of motion. Since the spot diameter and velocity of the flying spot were measured, it is more convenient to express the radiant exposure as a function of exposure time τ.

With

$$v = \frac{2\omega_0}{\tau} = \frac{d_0}{\tau}, \tag{2}$$

it follows that

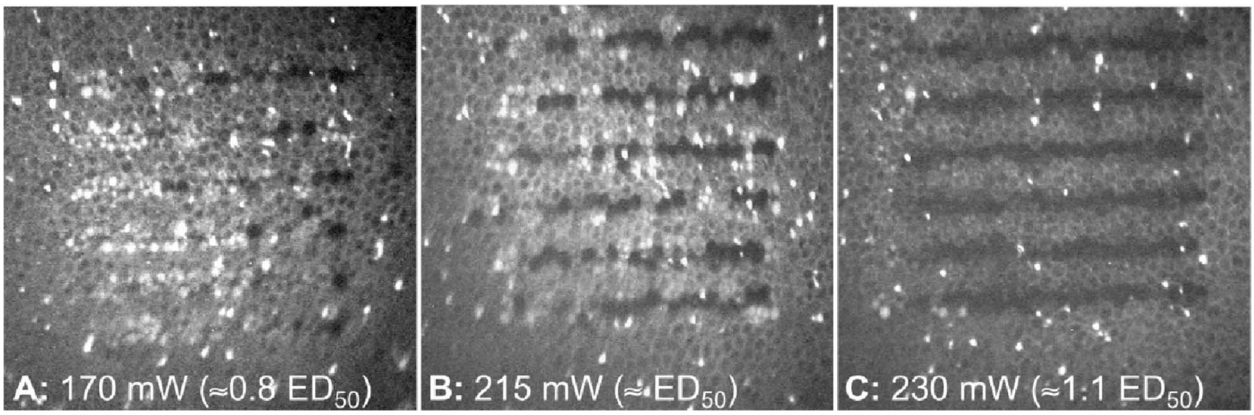

Fig. 6 Calcein fluorescence images after irradiation with 3 μs (all 10 repetitions with 100 Hz). Power increases from (a) to (c). Below ED_{50}, (a) few exposed cells are damaged. At about ED_{50}, (b) lines of dead cells are one or two cells wide; not all cells are damaged. Above ED_{50}, (c) all exposed cells were damaged and widening of the lines was observed. Clearly separated lines of dead cells, resembling the applied scan pattern, suggest selectivity of the method within the RPE monolayer.

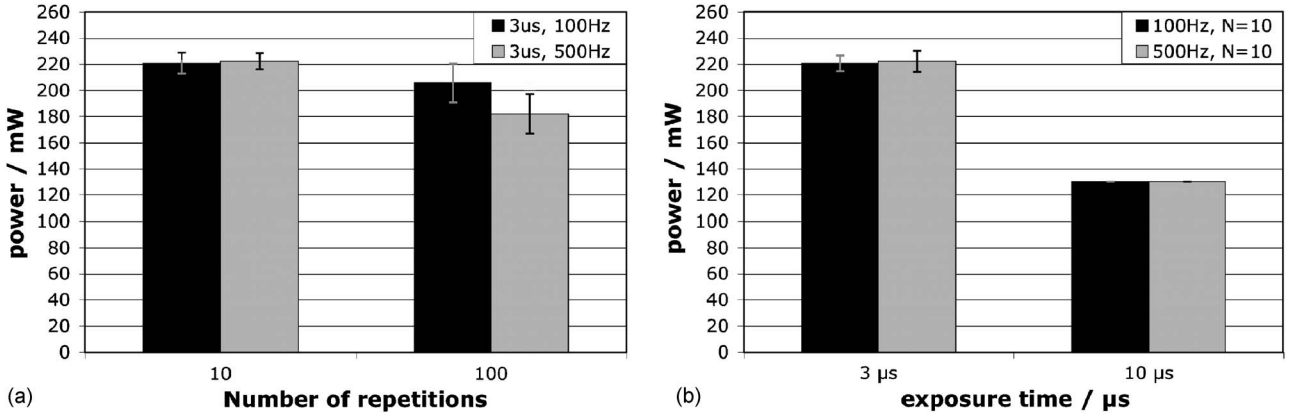

Fig. 7 Summary of *in vitro* experiments. (a) ED_{50} power reduced with the number of repetitions applied to each treatment site as shown for 3-μs exposures at 100 and 500 Hz. (b) ED_{50} reduced with exposure time as shown for 10 repetitive exposures. All measurements were performed in duplicates. Therefore, the data points are the average ED_{50}, and error bars represent the absolute deviation.

$$H(y) = \sqrt{\frac{2}{\pi}} \cdot \frac{2 \cdot P \cdot \tau}{d_0^2} \cdot \exp\left(-\frac{2y^2}{\omega_0^2}\right). \tag{3}$$

Consequently, each melanosome on the scan axis experiences a radiant exposure of

$$H(0) = \sqrt{\frac{2}{\pi}} \cdot \frac{2 \cdot P \cdot \tau}{d_0^2}. \tag{4}$$

Thus, cell damage radiant exposure is evaluated from the cell damage power.

3 Results

Careful design of both the *in vitro* and *in vivo* scanners ensured a constant scan speed across the scan line, nearly Gaussian irradiance profile, and a large depth of focus. Due to the small scan angle necessary to create the desired size of the scan pattern and the telecentric placement of the focusing lens, aberrations caused by scanning were not observed. The scan speed was measured to be constant along the line for both devices (Fig. 5). No-F Theta effects were observed, that is, the velocity of the flying spot is not larger toward the edges of the scan field than it is in the center.

3.1 *In Vitro Experiments*

With the knife-edge method, the spot diameter on the sample was measured to be 20 μm. The scan field was nearly square with a length of the scan lines and a height of the pattern of 300 μm.

Selective damage of RPE cells is feasible using a laser scanning device that employs a Gaussian laser beam. Calcein viability assay performed after irradiation showed separate lines of dark cells in the fluorescence images, resembling the applied scan pattern. Close to ED_{50}, the widths of these lines were one or two RPE cells thick. Cells in between the scan lines remained viable, suggesting selectivity within the RPE monolayer (Fig. 6).

The ED_{50} power for cell damage decreased with the increase of the number of scans from 10 to 100 repetitive exposures [Fig. 7(a)]. Increasing the dwell time from 3 to 10 μs (i.e., slowing down the velocity of the flying spot) also decreased the necessary power to damage the cells [Fig. 7(b)]. The slopes of the dose response of individual samples were all smaller than 1.1 (Table 1).

Morphological changes were not observed under white light illumination except at power levels significantly above threshold; they were more likely to be seen when scans were performed with 500-Hz repetition frequency. A dependence of the ED_{50} on the repetition frequency was not observed. However, reversible shrinking of the tissue occurred during irradiation with 500-Hz repetition frequency, when the sample was exposed to power levels three times above the damage threshold (ED_{50}) while scanning 100 repetitive 10-μs exposures.

3.2 *In Vivo Experiments*

3.2.1 *Scanner characterization*

The $1/e^2$ spot diameter was measured, by means of detecting the rise and fall time of the rotating knife edge, to be 27.5 μm in air (Fig. 8). The spot size on the rabbit retina was calculated to be 18 μm after taking into account the Goldman contact lens and the optics of the rabbit eye.[18] Differentiation of the rise and fall time signals from the knife-edge measurement suggested that the beam was nearly Gaussian (Fig. 9). Discrepancy between the calculated diffraction-limited spot diameter of 19.2 μm and measured real diameter of 27.5 μm indicates a times-diffraction-limit factor M^2 of about 1.4.

Translation of the rotating knife edge in small increments through the beam waist along the optical axis led also to determination of the beam propagation around the focus. In our device, the irradiance applied to the target site varied by only 10% over a range of ±200 μm on either side of the focus (Fig. 8). The long depth of focus is the result of system design that uses low numerical aperture optics.

3.2.2 ED_{50} *Threshold determination*

RPE cells can be damaged selectively *in vivo* as indicated by leakage of the fluorescein dye in the form of the scan pattern with concurrent lack of visible coagulation of the neurosensory retina. Figure 10(a) is a fundus photograph of a rabbit minutes after irradiation. Two columns of marker lesions that

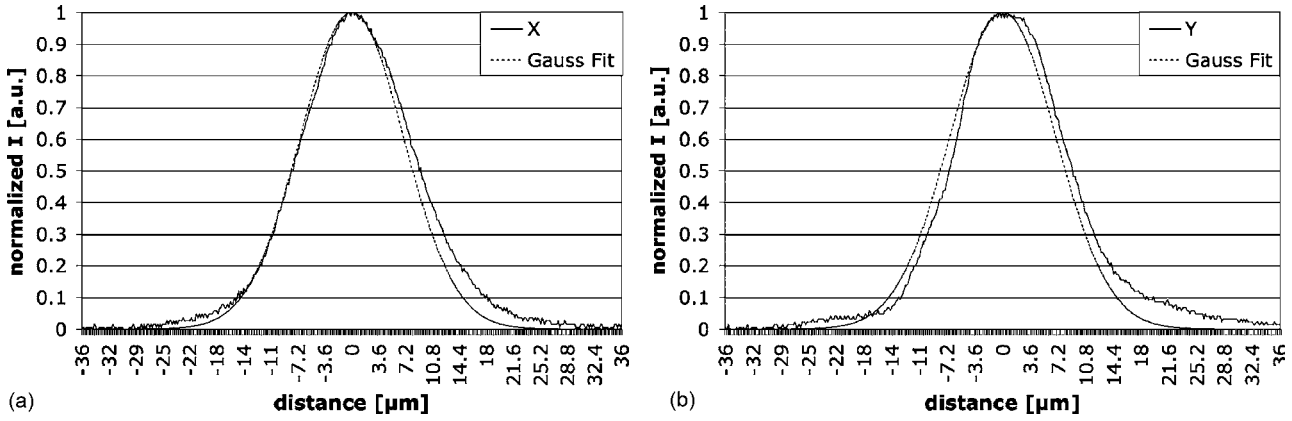

Fig. 8 Beam profile in air along (a)=x and perpendicular (b)=y to the direction of motion of the spot in the focal plane. The beam is 27.5 μm in diameter with a nearly Gaussian irradiance profile. Ratio of the measured spot diameter ($1/e^2$) of 27.5 μm over a calculated diffraction-limited diameter of 19.2 μm indicates M^2 of 1.4.

served as orientation points are visible. Selective lesions were placed between columns of markers and were ophthalmoscopically not visible (i.e., no retinal whitening) [Fig. 10(a)]. Ophthalmoscopically invisible lesions can be visualized by fundus angiography, where fluorescein can pool into the eye in those areas, where the blood ocular barrier has been compromised by laser mediated RPE cell damage. Thus, Fig. 10(b) shows the fluorescence image of the same site of Fig. 10(a) one hour post irradiation. Here, the marker lesions appear dark in the center with a bright rim, and previously nonvisible selective lesions show up as hyperfluorescent. Thus, angiographic ED_{50} was determined by the angiographic visibility of lesions.

For the separated lines scan pattern, the cell damage ED_{50} decreased with exposure time from 93 mW with 7.5-μs to 66 mW with 15-μs exposure. This corresponds to an increase of the ED_{50} radiant exposure from 340 mJ/cm^2 to 482 mJ/cm^2 (Fig. 11). ED_{50} (both in terms of power and radiant exposure) also decreased with increasing number of exposures. With the available maximum power of the system, we were not able to reach the ophthalmoscopic damage threshold, as indicated by visible retinal coagulation, for all irradiation parameters except for 100 repetitions of 15-μs exposures with an interlaced scan pattern (Fig. 11 and Table 3).

Irradiating with the INT scan pattern, which uses interlacing lines without spacing between lines, reduced the threshold power required for cell damage compared to separated lines (Table 3). Ophthalmoscopic threshold was reached for the most "invasive" parameter used—100 repetitions with 15-μs exposure time. For this case, the ophthalmoscopic ED_{50} was 1.7 times the angiographic ED_{50}. The ratio of ophthalmoscopic ED_{50} over angiographic ED_{50} is commonly referred to as the therapeutic window (TW).

The Probit slopes for all individual eyes were smaller than 1.1, indicating a steep dose response of the irradiated cells (Table 2).

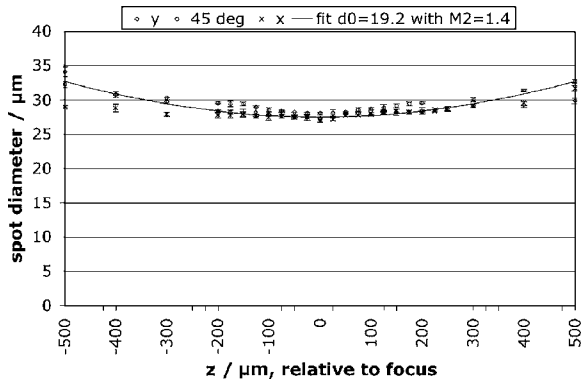

Fig. 9 Beam diameter around the focus of the system derived from the rotating knife-edge measurements. Data were fit to diffraction-limited beam propagation considering an M^2 of 1.4. With this beam propagation, irradiance varies by only 10% over a distance of +/−200 μm around the focus.

4 Discussion

We have developed an acousto-optic laser scanner and tested its feasibility for selective targeting of the RPE *in vitro* and *in*

Table 3 Dependence of angiographic ED_{50} and therapeutic window (TW) on the scan pattern applied [interlaced lines (INT) versus separated lines (SEP)]. For 7.5-μs exposures, no visible coagulation of retinal tissue was achieved with the maximally available power of 185 mW. For 15 μs, using the interlacing scan pattern, retinal whitening occurred at a power of a factor 1.7 higher than the angiographic ED_{50}. For the same exposure time applied through the SEP scan pattern, we were not able to coagulate photoreceptors; our maximal available power of 185 mW is a factor of 3.2 higher than the angiographic ED_{50} of that set of parameters. Thus, the therapeutic window for this case would be larger than 3.2.

Parameter	Angiographic ED_{50} (mW)	Ophth. ED_{50} (mW)	TW
7.5 μs, N=10, SEP	92	(>180)	—
7.5 μs, N=10, INT	69	(>18)	—
15 μs, N=100, SEP	57	(>18)	(>3.2)
15 μs, N=100, INT	45	=75	1.7

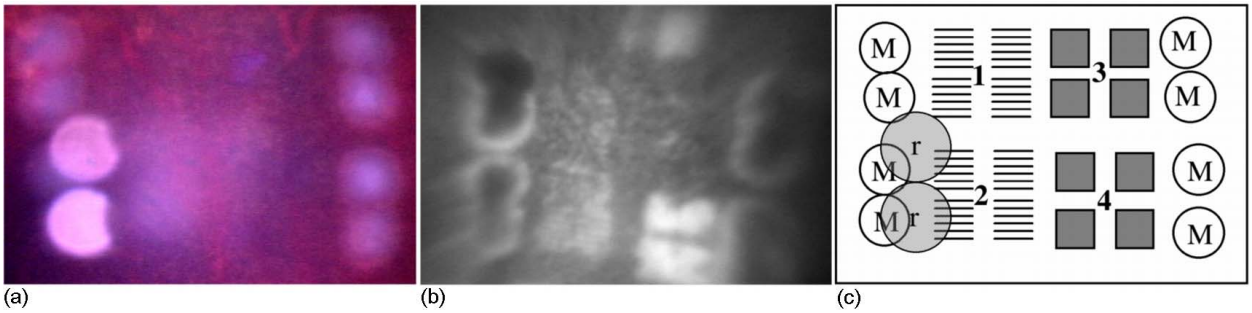

Fig. 10 View through the slit lamp (a) minutes after irradiation and corresponding fluorescence angiographic image (b) taken 1 h after irradiation of the same site with (c) additional corresponding sketch of the site. Selective lesions were placed between marker lesions (M), in which photoreceptors have been purposely coagulated by applying a very slow scan speed. Selective 7.5-μs exposures using separate lines were performed at (1) $1\times ED_{50}$ and (2) $2\times ED_{50}$, and with interlaced lines also at (3) 1 ED_{50} and (4) 2 times ED_{50}. (a) All selective lesions were ophthalmoscopically invisible minutes post irradiation—the view in the lower left side of the image is partially obstructed by reflections (r) of the double-slit illumination from the contact lens. (b) Selective lesions become visible in fluorescence angiography as separated hyperfluorescent lines, where irradiation had been performed with the SEP scan pattern. Lesions close to the right column of markers were produced using the INT scan pattern; consequently, no separate fluorescence is visible.

vivo. Selectivity is achieved by rapid scanning of the focused spot from a cw solid-state green laser to create microsecond exposure at each RPE cell. Careful design ensured a nearly Gaussian profile for irradiation and a large depth of focus. The spot diameter was 20 μm for the *in vitro* bench-top device and 27.5 μm in air for the slit-lamp adapted *in vivo* scanner. In the rabbit eye, the spot size was calculated to be 18 μm, due to the optics of the rabbit eye. The large depth of focus ensures that the irradiance on the RPE does not vary significantly with small change in focusing conditions, an important consideration because precise focusing is not always achieved in a clinical setting. *In vitro* experiments were performed on prepared sheets of young bovine RPE, where the neurosensory retina was peeled off. *In vivo* experiments were performed on Dutch belted rabbits.

4.1 *In Vitro Experiments*

In vitro results showed that it is possible to selectively destroy RPE cells by means of a scanned cw laser spot with a Gaussian irradiance profile. Selectivity is demonstrated by alternating lines of dead and surviving cells that resemble the applied scan pattern (Fig. 6). The ED_{50} power decreased with increasing exposure time [Fig. 7(b)]. This is expected, as more energy is deposited in the tissue, the longer the laser radiation is applied. ED_{50} power in addition decreased with the increasing number of repetitive exposures applied to the irradiation site [Fig. 7(a)]. No significant difference in ED_{50} between the tested repetition frequencies of 100 and 500 Hz was found. However, morphological changes that are visible even without fluorescence illumination seemed to be more likely to appear with 500-Hz repetition frequency. In addition, shrinking of the tissue was observed at a factor of about 3 above ED_{50} for 10-μs exposures at a repetition frequency of 500 Hz, suggesting that this combination of parameters leads to significant background temperature increase. Consequently, all *in vivo* experiments were performed at 100-Hz repetition frequency.

4.2 *In Vivo Experiments*

In vivo experiments in rabbits demonstrated that RPE cells can be damaged selectively, as shown by fluorescein leakage that resembles the scan pattern with concurrent absence of ophthalmoscopically visible coagulation. RPE cell damage was achieved with moderate laser power ($<$100 mW). For the most invasive parameter, the therapeutic window is 1.7. The fact that we were not able to visibly coagulate neurosensory retina with all other parameters suggests that the therapeutic window is larger for those cases.

The angiographic ED_{50} power decreased with increasing dwell time. At the same time, the ED_{50} radiant exposure increased. As the dwell time increasingly exceeds the thermal confinement time of the RPE cells ($\sim$5 μs), more energy has to be applied to compensate for heat diffusion.

Surprisingly, we were not able to visibly coagulate the neurosensory retina with our maximal available power of 185 mW when applying the SEP scan pattern, even for an exposure time of 15 μsec, which exceeds the thermal relaxation time of the RPE. This can be explained by the small spot of irradiation. When a single RPE cell is exposed, heat diffusion can occur in three dimensions. Even when a line is irradiated, 2-D heat diffusion away from the cylinder is more efficient than when a large area of RPE is irradiated at a time. In the latter case, heat can only diffuse axially, leading to higher temperature at the neurosensory retina.

Heat diffusion also explains why the threshold for the interlacing lines (INT) scan pattern is lower than for the SEP pattern for the same scan speed. In the most extreme case, we were able to visibly coagulate the neural retina by applying 100 repetitions of the INT pattern with 15-μs exposure time at a factor of 1.7 above ED_{50} (Table 3). In the interlaced lines scan pattern, adjacent lines are created with a time delay of 3 ms. During this time, cells adjacent to the first line of the pattern will have been heated by heat diffusion from the exposed, neighboring cells, so that the returning spot adds its energy to their already increased temperature. In addition, the duty cycle of the interlace pattern is well above 50%, so that the heating approaches a 2-D sheet rather than separated cylinders. Thus, heat diffusion into the neural retina is more pronounced than it would be with the separated line scan pattern.

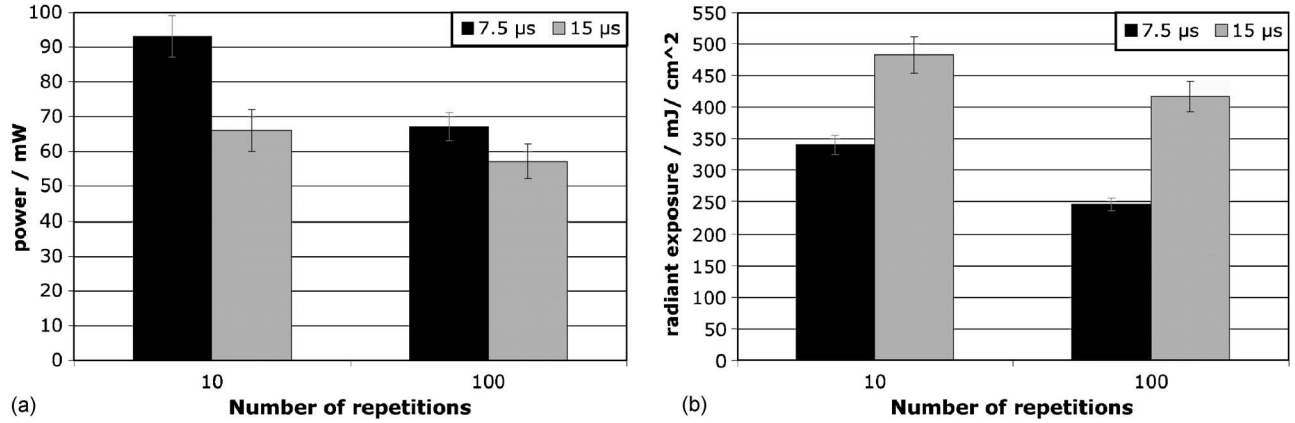

Fig. 11 Influence of the exposure time and the number of exposures of the SEP pattern on (a) the angiographic ED_{50} power and (b) ED_{50} radiant exposure. Angiographic ED_{50} radiant exposures were calculated using Eq. (4). All measurements were performed in duplicates. Therefore, the data points are the average ED_{50} and error bars represent the absolute deviation. Ophthalmoscopically visible lesions could not be produced for these parameters with laser power of up to 185 mW.

4.3 *Cell Damage Mechanism*

The mechanism for selective RPE cell damage was originally thought to be thermal damage.[8] Lin and Kelly were able to show that formation of microbubbles around the melanosomes is the main mode of cell killing for pico- and nanosecond pulses. They found that a single formation of a microbubble might be sufficient for cell killing.[20,21] Brinkmann et al. demonstrated that cell damage by 3-μs pulses originates from bubble formation around melanosomes that ruptures the cell structure.[22] Roegener, Brinkmann, and Lin verified that RPE cells died when a single bubble was detected within a train of 6-μs-long pulses.[23] Schuele et al. demonstrated, using an opto-acoustic technique, that cells are damaged mainly by cavitation for 5-μs exposures, while for 500-μs pulses, all cells die without formation of intracellular microbubbles. He detected a mixed damage effect for 50-μs exposures, with most cells being killed without microbubble formation.[24] In a related project, we measured bubble formation by detection of backscattered irradiation light, and found it to be the predominant cell damage mechanism for pulse durations up to 20 μs.[25]

These bubbles are small cavitation events that are confined to the vicinity of the absorbers near the center of the scan line where the temperature is highest.[15] At threshold, the mechanical stress caused by expansion and rapidly ensuing collapse of the microbubbles is capable of rupturing the cell membrane or damaging intracellular organelles, which subsequently leads to cell death. They are, however, not capable of destroying Bruch's membrane or photoreceptors. In our experiments, this is indicated *in vitro* by loss of Calcein fluorescence and an unaltered morphological appearance of the cells after exposure. *In vivo* subtle damage to the RPE layer manifests itself in fluorescein leakage with concurrent absence of visible photoreceptor damage and absence of bleeding from the choriocapillaris into the ocular space. Roider et al. demonstrated by means of microperimetry in a clinical study that no blind spots appeared due to the laser treatment,[13] which means that photoreceptor function has not been compromised by either bubble formation or heat diffusion.

4.4 *Outlook*

Our results suggest that controlled injury of the RPE cells can be achieved using a laser scanning device without thermal coagulation of the retina. A scanning device can be made more compact and less expensive than the existing system that generates multiple pulse trains. The required (cw) laser power is moderate, allowing for future treatment devices to be built with a solid-state laser source mounted directly on a slit lamp. Furthermore, the scanning approach is more versatile compared to any pulsed approach, because a variety of scan patterns and scan parameters can be performed under software control. By adjusting the scanning speed, it is even possible to perform both selective targeting and conventional (nonselective) laser coagulation using the same device, as we have shown by placing ophthalmoscopically visible marker lesions in the rabbit fundus using reduced scanning speeds.

With our current setup, power delivery to the eye was limited to 185 mW due to the use of a single-mode fiber. As a consequence, exposure time was limited to relatively long exposures. Future setups will incorporate a compact laser source of about 1-W output power mounted directly onto the slit lamp. This will allow for higher power to be delivered to the eye and thus enable exploration of shorter exposure times. Additionally, it will alleviate the need for single-mode fiber coupling and make the setup more robust. For patient treatment, an active feedback device that monitors proper function of the scanning process will be required to avoid overexposure of the eye in case of a failure of the scanner. However, we note that for AO scanners, most likely failure modes will result in the absence of the first-order laser beam, and therefore no light will reach the eye.

As mentioned in the Introduction, the actual treatment effect is presumably achieved by the regeneration of RPE cells to form a new, healthy blood retinal barrier. Although lesions created by the SEP scanning pattern can be expected to heal faster because of the presence of viable cells between the scan lines, further studies are needed to determine whether the smaller total number of cells damaged by the SEP pattern is sufficient for treating symptoms such as an existing edema or

drusen. In addition, histological examination is needed to verify whether the absence of visible retinal coagulation means that the outer segments of the photoreceptors are indeed intact. These studies are currently underway.

Due to the small diameter of the spot, dosimetry and accurate focusing in a clinical setting are crucial. Our scanning device was designed to create a long depth of focus. Using a NA of 0.02, focusing inaccuracies of 200 and 500 μm lead to a loss of irradiance of only 10 and 30%, respectively, in our scanner (Fig. 9). In our rabbit experiments, focusing was not a problem as long as irradiation was performed in the central region of the fundus, where selective treatment is most useful. Due to the expected large therapeutic window, treatment in a clinical setting can be performed well above ED_{50}. However, to ensure efficient and safe treatment in a clinical setting, immediate feedback over the treatment outcome is desirable. At present, treatment outcome is assessed with fluorescence angiography one hour post-irradiation. We are currently developing a system that monitors cell death during treatment by detecting bubble formation, alerting the physician when the endpoint is reached.

5 Conclusions

Selective destruction of RPE cells is feasible *in vitro* and *in vivo* using laser scanning devices, which utilize Gaussian beams. Sheets of young bovine RPE cells are selectively damaged with laser power of about 200 mW for 3 and 10 μs exposure times. *In vivo* in Dutch belted rabbits, we find an ED_{50} below 100 mW for exposure times of 7.5 μs and longer. In both *in vitro* and *in vivo* experiments, we find the cell damage ED_{50} power to decrease with exposure time and number of repetitions applied to the treatment site. *In vivo* applying an interlacing lines scan pattern also reduces the ED_{50}.

We demonstrate selectivity by alternating lines of surviving and dead cells *in vitro* and *in vivo* and by absence of retinal whitening *in vivo*. We identify lesions by fluorescence angiography after *in vivo* experiments, which show separate fluorescent lines that resembled the scan pattern. The extent of selectivity for various parameters, however, has to be determined by histological examination.

We consider a scanning device an attractive future alternative to conventional laser coagulation and pulsed repetitive targeting of the RPE.

Acknowledgment

This work has been supported by the National Institutes of Health (NIH EY 12970) and Lumenis, Incorporated.

References

1. R. Birngruber, "Die Lichtbelastung unbehandelter Netzhautareale bei der Photokoagulation," *Fortschr. Ophthalmol.* **81**, 147–149 (1984).
2. B. Lorenz, R. Birngruber, and A. Vogel, "Quantifizierung der Wellenlängenabhängigkeit laserinduzierter Aderhauteffekte," *Fortschr. Ophthalmol.* **86**, 644–654 (1989).
3. J. Marshall and J. Mellerio, "Pathological development of retinal laser photocoagulations," *Exp. Eye Res.* **7**, 225–230 (1968).
4. I. H. Wallow, R. Birngruber, V. P. Gabel, F. Hillenkamp, and O. E. Lund, "Netzhautreaktion nach intensivlichtbestrahlung," *Adv. Ophthalmol.* **31**, 159–232 (1975).
5. P. Tornquist, A. Alm, and A. Bill, "Permeability of ocular vessels and transport across the blood-retinal-barrier," *Eye* **4**, 303–309 (1990).
6. I. Grierson, P. Hiscott, P. Hogg, H. Robey, A. Mazure, and G. Larkin, "Development, repair and regeneration of the retinal pigment epithelium," *Eye* **8**, 255–262 (1994).
7. N. Bulow, "The process of wound healing of the avascular outer layers of the retina. Light- and electron microscopic studies on laser lesions of monkey eyes," *Acta Ophthalmol. Suppl.* **139**, 7–60 (1978).
8. J. Roider, N. A. Michaud, T. J. Flotte, and R. Birngruber, "Response of the retinal pigment epithelium to selective photocoagulation," *Arch. Ophthalmol. (Chicago)* **110**, 1786–1792 (1992).
9. R. R. Anderson and J. A. Parrish, "Selective photothermolysis: precise microsurgery by selective absorption of pulsed radiation," *Science* **220**, 524–527 (1983).
10. V. P. Gabel, R. Birngruber, and F. Hillenkamp, "Visible and near infrared light absorption in pigment epithelium and choroid," in *Intl. Congress Series No. 450, XXIII Concilium Ophthalmologicum*, K. Shimizu, Ed., *Excerpta Medica*, pp. 658–662 (1978).
11. J. Roider, F. Hillenkamp, T. J. Flotte, and R. Birngruber, "Microphotocoagulation: Selective effects of repetitive short laser pulses," *Proc. Natl. Acad. Sci. U.S.A.* **90**, 8643–8647 (1993).
12. J. Roider, R. Brinkmann, C. Wirbelauer, H. Laqua, and R. Birngruber, "Subthreshold (retinal pigment epithelium) photocoagulation in macular diseases: a pilot study," *Br. J. Ophthamol.* **84**, 40–47 (2000).
13. J. Roider, R. Brinkmann, C. Wirbelauer, H. Laqua, and R. Birngruber, "Retinal sparing by selective retinal pigment epithelial photocoagulation," *Arch. Ophthalmol. (Chicago)* **117**, 1028–1034 (1999).
14. C. Framme, G. Schüle, J. Roider, D. Kracht, R. Birngruber, and R. Brinkmann, "Threshold determinations for selective retinal pigment epithelium damage with repetitive pulsed microsecond laser systems in rabbits," *Ophthalmic Surg. Lasers* **33**(5), 400–409 (2002).
15. R. Brinkmann, N. Koop, M. Oezdemir, C. Alt, G. Schüle, C. P. Lin, and R. Birngruber, "Targeting of the retinal pigment epithelium (RPE) by means of a rapidly scanned continuous wave (CW) laser beam," *Lasers Surg. Med.* **32**, 252–264 (2003).
16. D. H. Sliney, J. Mellerio, V. P. Gabel, and K. Schulmeister, "What is the meaning of threshold in laser injury experiments? Implications for human exposure limits," *Health Phys.* **82**, 335–347 (2002).
17. Product Information, CalceinAM, Molecular Probes, Eugene, OR, www.molecularprobes.com (2002).
18. R. Birngruber, F. Hillenkamp, and V. P. Gabel, "Experimentelle und theoretische untersuchungen zur thermischen schädigung des augenhintergrundes durch laserstrahlung," *GSF-Report*, AO251, Gesellschaft für Strahlen- und Umweltforschung m.b.H., München (1978).
19. R. G. Borland, D. H. Brennan, J. Marshall, and J. P. Viveash, "The role of fluorescein angiography in the detection of laser-induced damage to the retina: A threshold study for Q-switched, Neodymium and Ruby lasers," *Exp. Eye Res.* **27**, 471–493 (1978).
20. W. M. Kelly, and C. P. Lin, "Microcavitation and cell injury in RPE following short-pulsed laser irradiation," *Proc. SPIE* **2975**, 174–179 (1997).
21. C. P. Lin and W. M. Kelly, "Cavitation and acoustic emission around laser heated microparticles," *Appl. Phys. Lett.* **72**, 2800–2802 (1998).
22. R. Brinkmann, G. Hüttmann, J. Rögener, J. Roider, R. Birngruber, and C. P. Lin, "Origin of retinal pigment epithelium cell damage by pulsed laser irradiance in the nanosecond to microsecond time regimen," *Lasers Surg. Med.* **27**, 451–464 (2000).
23. J. Rögener, R. Brinkmann, and C. P. Lin, "Pump-probe detection of laser-induced microbubble formation in retinal pigment epithelium cells," *J. Biomed. Opt.* **9**, 367–371 (2004).
24. G. Schuele, M. Ruhmor, G. Huettmann, and R. Brinkmann, "RPE damage thresholds and mechanisms for laser exposure in the microsecond-to-milllisecond time regimen," *Invest. Ophthalmol. Visual Sci.* **46**, 714–719 (2005).
25. H. Lee, C. Alt, C. M. Pitsillides, and C. P. Lin, "Reflectometric detection of intracellular cavitation during selective targeting of the retinal pigment epithelium: dependence of cell death mechanism on pulse detection," (manuscript in preparation).